PAPER • **OPEN ACCESS**

Spatial resolution limits of EPMA

To cite this article: B Buse and S L Kearns 2020 *IOP Conf. Ser.: Mater. Sci. Eng.* **891** 012005

IOP Conf. Series: Materials Science and Engineering **891** (2020) 012005 doi:10.1088/1757-899X/891/1/012005

Spatial resolution limits of EPMA

B Buse and S L. Kearns

University of Bristol, School of Earth Sciences, Wills Memorial bldg., Queen's Road, Bristol BS8 1RJ, Great Britain

e-mail: ben.buse@bristol.ac.uk

Abstract. The development of field emission EPMA, has significantly improved the lateral resolution of EPMA. Two strategies are available for achieving high spatial resolution, either low overvoltage or low voltage analysis. Determining the spatial resolution for a particular analysis is complex and depends on the voltage, spot size, beam current, density of the sample, X-rays analysed and the precision and sensitivity required. Monte carlo simulations can be used to evaluate the spatial resolution for different analytical conditions and samples, provided the minimum spot size achievable at the conditions is known. Spot size is important in determining lateral resolution, which initially improves with decreasing accelerating voltages, and then increases as the minimum spot size becomes more significant than the distance electrons travel. For trace elements, the requirement for precision and sensitivity demands either higher overvoltages increasing the volume from which X-rays are generated, and/or higher beam currents increasing the spot size. At low overvoltage or low voltage conditions many additional factors must be considered: carbon contamination, coat thickness, erosion of the carbon coat, the stability of the sample and the problems surrounding the measurement of soft X-ray lines including L-lines for first row transition metals. When analysing L-lines for quantifying first row transition metals, either calibration curves must be used, or the anomalous mass absorption and variations in the fluorescence yields from partial shell occupancy must be accounted for, by using fits to experimentally determined values. By taking these factors into consideration, high quality measurements can be performed.

1. Introduction

Electron probe microanalysis (EPMA) has traditionally employed a thermionic tungsten source analysing material on the scale of several cubic micrometres (for densities of 2 - 5 g/cm^3), at accelerating voltages of 15 - 20 kV. Field emission gun (FEG) EPMA, which employs a sharpened tungsten crystal to reduce the source area of electron emission and provides a dense beam of electrons, permits higher spatial resolution to be achieved at low voltage [1]. High spatial resolution is important for analysing small phases or inclusions, diffusion profiles and particles, although geometry must be considered for the latter. Monte Carlo simulation is often used to image the scattering and deceleration of the electron beam on entering a material. At high accelerating voltages (15 - 20 kV) the electron range (the distance electrons travel into the sample) is several microns (Fig. 1) whilst the beam diameter (spot size) is comparatively small (10's - 100's nm) even for a conventional tungsten source. At low accelerating voltages (< 10 kV) the electron range is 100's nm (Fig. 1), making the spot size (10's - 100's nm) an important component of the lateral resolution (Fig. 2), exacerbated by the increase in beam diameter at lower accelerating voltages [1].

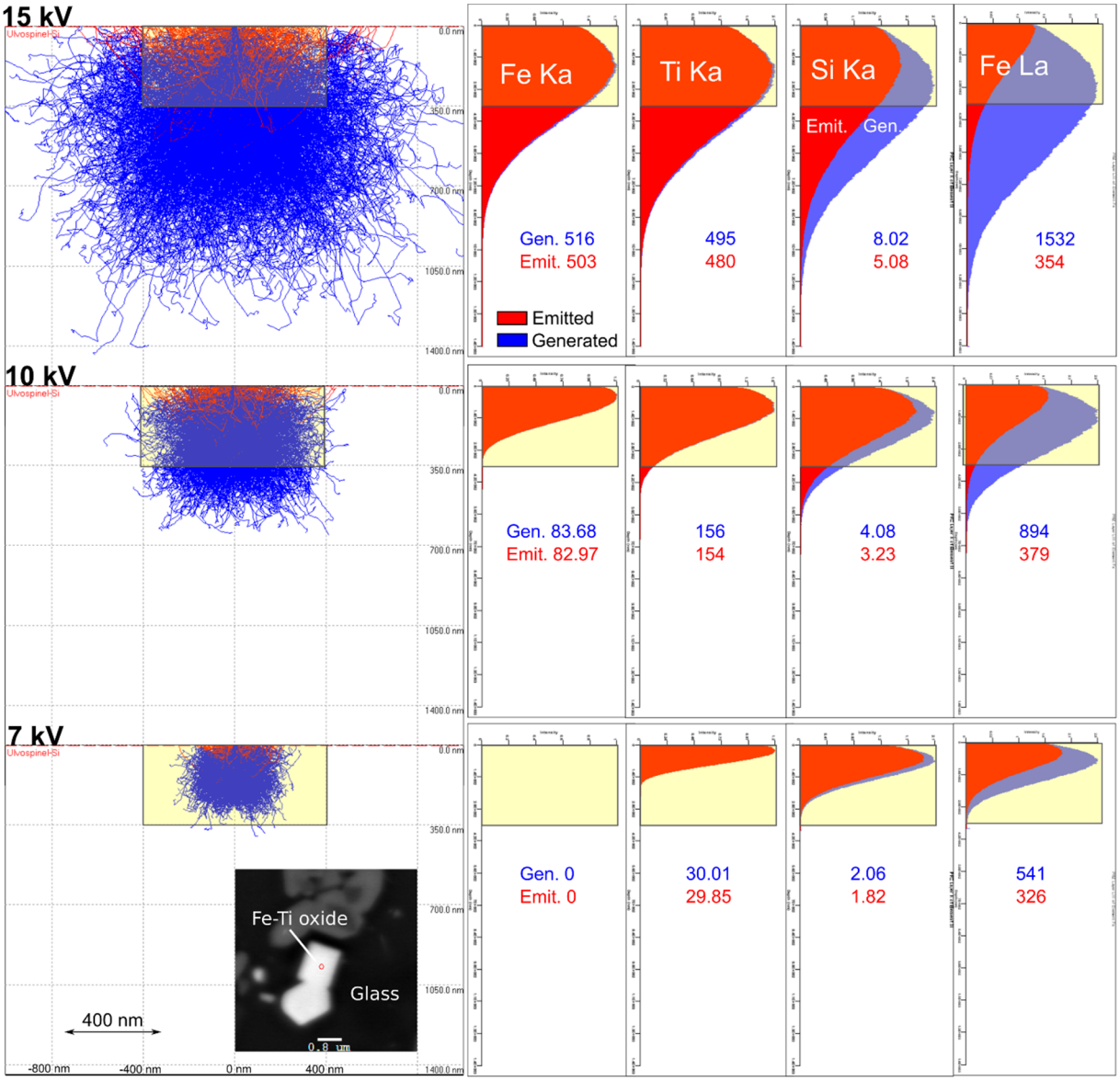

Figure 1. Monte Carlo simulations (using CASINO [2]) for bulk ulvospinel (Fe_2TiO_4) with trace Si and a density of 4.78 g/cm^3 for a beam diameter of 10 nm. On the left is the electron distribution, with backscattered electrons coloured red; on the right are the phi-rho-z curves for different elements. The blue and red values refer to the number of X-rays generated (Gen.) and emitted (Emit.) respectively. The yellow box represents the size of a 800 x 350 nm crystal, a typical size of minerals formed during high pressure experiments; see BSE image insert. Table 1 gives analyses for this crystal.

Pinard and Richter [3] and McSwiggen [4] have well characterised the interaction volume for a focussed beam as the accelerating voltage is reduced for FEG-EPMA at a constant beam current. The interaction volume initially reduces and then increases reflecting the interplay of electron range and spot size, with reduced accelerating voltage resulting in the electron range decreasing whilst spot size is increasing. Minimum interaction volumes were found to be typically in the 5 - 8 kV range. This may be calculated using Monte Carlo simulations for a range of beam currents, if the change in spot size with beam current and accelerating voltage is known, allowing the detection limit and precision to be considered and therefore the ability for trace elements to be measured at a given spatial resolution.

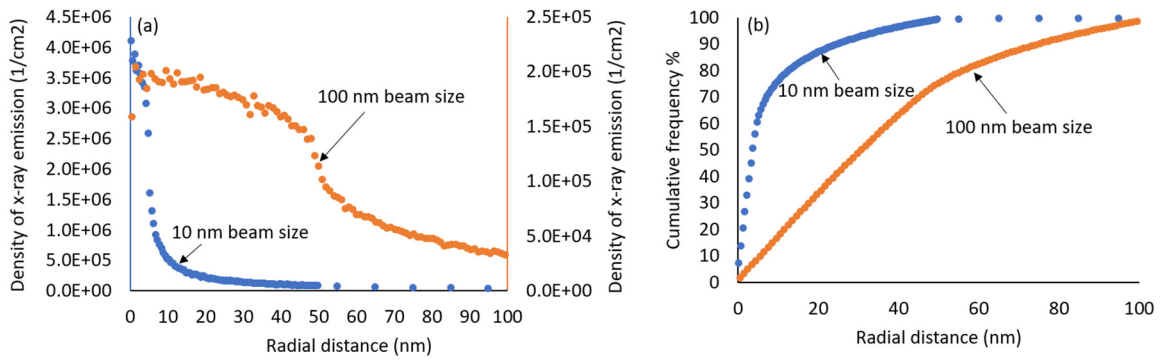

Figure 2. Fe-Lα radial distribution of X-rays calculated using PENEPMA Monte Carlo simulation [5] for ulvospinel at 7 kV and spot sizes of 10 nm and 100 nm.

Pinard and Richter [3] and McSwiggen [4] instead of considering the electron range and electron interaction volume, consider the volume from which X-rays are emitted. This determines the spatial resolution of chemical analysis and is termed 'analytical volume' by McSwiggen [4]. Given that different X-rays have different critical excitation energies at a single accelerating voltage, different X-rays will have different analytical volumes. If the overvoltage (the ratio of accelerating voltage to the critical excitation energy of the X-ray) is small, X-rays are generated close to the point at which the electron beam enters the sample (e.g., Fe Kα at 10 kV, Fig. 3). The low overvoltage means that only a small loss of energy is required before the beam is unable to excite the X-ray of interest. Whereas if the overvoltage is large, the analytical volume will closely correspond to the electron interaction volume (e.g., Si Kα at 10 kV, Fig. 3). The depth of the analytical volume is also dependent on the amount of absorption of the X-ray by the sample, determined by the mass absorption coefficient (MAC); in the case of oxygen Kα or Fe Lα which are soft X-rays (< 1 keV) and have high MACs only those X-rays generated near the surface are emitted and detected (e.g., Fe Lα at 20 kV, Fig. 3). This however has little effect on the lateral width of the analytical volume.

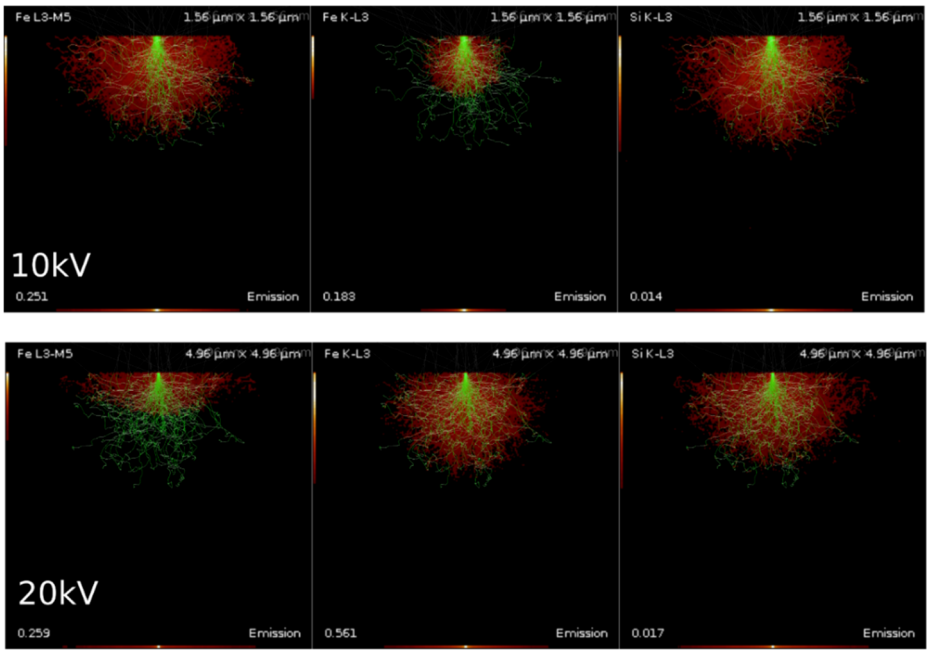

Figure 3. Integrated 2D X-Z slices displaying the source of emitted x-rays generated from Monte Carlo simulations using DTSA2 [6]. Red dots represent sites at which emitted X-rays are generated, green lines trace the electron trajectories.

1.1. Strategies for obtaining high spatial resolution

Two strategies are available for obtaining high spatial resolution in bulk samples (e.g., [3, 4, 7]; see [8] for very thin samples), either a low voltage resulting in a small electron interaction volume or a low overvoltage, which may be at relatively high accelerating voltage for a high energy X-ray, resulting in a small analytical volume for the X-ray of interest. Using low accelerating voltages allows multiple X-rays to be measured at a single accelerating voltage, with spatial resolution equal to or less than that of the interaction volume. In the example of the 350 nm thick ulvospinel in Fig. 1, all the elements could be analysed at 7 kV. Low voltage, however, limits the X-rays that are excited (e.g., Fe-L rather than Fe-K at 7 kV), often restricting the analyst to soft X-rays, which may be problematic. Problems include the close spacing of X-rays with the potential for peak overlaps, X-ray peaks may be subject to shifts and peak shape changes for different compounds (e.g., K-lines of B, C ,N and O [9]) or axial orientation (e.g., B-Kα [9]) and in the cases of Lα X-rays of first row transition metals and Mα X-rays of rare earth elements anomalous self absorption occurs (e.g., [10-12]). Surface layers also become significant, reducing the beam energy entering the sample and absorbing soft X-rays. The following must be considered: (1) thickness of conductive coat [13], including erosion of a carbon coat by the electron beam, where high current density is used (small beam size and high beam current) particularly at low accelerating voltages [14]; (2) presence of oxide layers on metal samples [15]; and (3) carbon contamination, commonly deposited in a ring around the electron beam (see Fig. 4) affecting closely spaced analyses [16, 17].

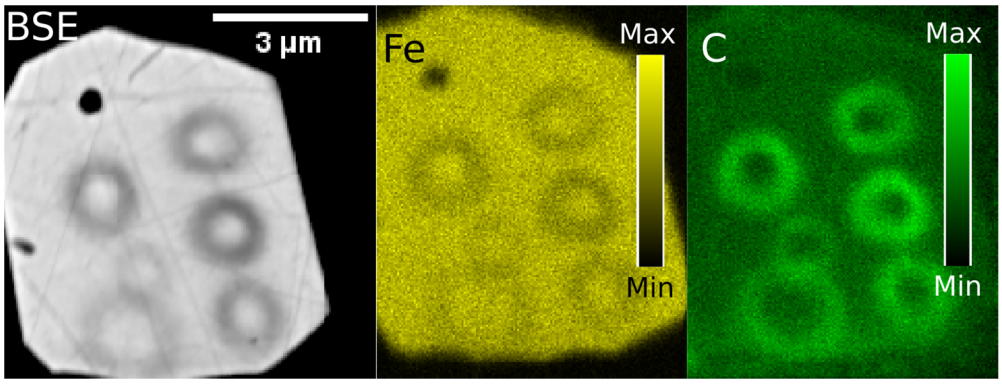

Figure 4. Backscatter electron (BSE) image and C and Fe X-ray intensity maps of analysis spots on a Fe-Ti spinel. Carbon contamination forms rings around the point of electron beam impact. At low overvoltage (accelerating voltage: 8.5 kV, critical excitation energy of Fe-Kα: 7.1 keV) carbon contamination strongly reduces Fe-Kα intensity.

Analysis at low overvoltage conditions at high voltages, avoids the necessity to use soft X-rays but low overvoltage conditions will only be satisfied for a few elements at a single voltage requiring multiple voltage analysis. In the example of the 350 nm Ulvospinel of Fig. 1, Fe Kα can be analysed at 10 kV, whilst Ti and Si must be analysed at 7 kV, to keep the analytical volume within the ulvospinel (see Table 1 for results). At low overvoltages surface layers (contamination, conductive coats, and oxide layers) become very significant (see figure 4, also [14, 17]), with a small reduction in beam energy entering the sample resulting in a large drop in X-rays generated.

Methods to mitigate the problems of surface layers include reducing carbon contamination by using liquid nitrogen or Peltier-cooled cold fingers (e.g., [17-19]), empirical correction [17], oxygen air jets for samples without a conductive carbon coat [18] and sample preparation by focussed ion beam (FIB) milling or cross-section polishing by Ar-ions to remove surface contaminations [20]. Recently for metal

Table 1. Quantification of a 800 nm wide ulvospinel in a Si-rich, Fe-poor glass at multiple voltages, using the Kα X-ray line for Fe. To achieve a reasonable quantification, Fe must be analysed at 10 kV, whilst the other elements analysed at 7 kV (see Fig. 1).

	MgO	SiO_2	CaO	FeO	Na_2O	Al_2O_3	K_2O	TiO_2	Total
15kV	1.24	26.37	0.71	59.15	1.13	6.47	0.72	11.39	107.15
10kV	1.29	4.73	0.18	76.48	0.04	1.64	0.09	15.47	99.90
7kV	1.32	1.36	0.24	76.48[a]	0.01	0.98	0.05	17.52	97.96

[a] 10 kV measurement used.

samples, Yamashita *et al.* [21] demonstrated the effectiveness of in-chamber plasma cleaning, sample heating together with a liquid nitrogen cold trap. Problems of the electron beam erosion of the carbon coat can be mitigated by: (1) reducing the current density, which may compromise either resolution or precision, (2) switching to a different conductive coat material, or (3) correcting for X-ray intensity change using time-dependent-correction (TDI) [14].

1.2. First row transition metal l-line analysis

For the analysis of many materials, first row transition metals are important. For low voltage analysis it may not be possible to excite the K-line X-rays, requiring analysis of the L-line X-rays. There has been considerable research exploring the complications in quantifying these lines. In 1985, Pouchou and Pichoir [22] demonstrated for Ni alloys, that the Lα X-rays suffered from anomalous self-absorption and partial fluorescence yields, with absorption varying not just with element concentration but the structure of the valance band, which is affected by the chemical environment (chemical bonding of atoms) requiring different MACs for different compositions. Similarly, the partial fluorescence yield varies with composition. Pouchou and Pouchoir [22] showed that for a binary series the MAC and partial fluorescence yield can be calculated using regression, allowing quantification. Fialin [23] noted the problem in MACs changing with electronic structure for Zn minerals and, therefore, standards and unknowns may have different MACs. More recently, Llovet *et al.* [24] applied this approach to Ni silicides, and Buse and Kearns [25] to olivines and showed that if solid-solution MACs and partial fluorescence yields are incorporated in matrix corrections, quantification is possible to an accuracy of ≤ 4 % relative. In examining olivines, Buse and Kearns [25] illustrated some of the difficulties in this approach; it requires measuring off-peak for some compositions and measuring the MAC across the absorption edge, where it is highly sensitive to the position of measurement. Moy and Fournelle [26] have instead of using conventional WDS peak and background measurements, have derived peak intensities through spectral deconvolution, from which MACs and partial fluorescence yields have been derived.

Remond *et al.* [27] tried a different approach to deal with anomalous absorption of Lα and Lβ, by acquiring spectra, from which absorption spectra were calculated and used to correct the spectra. Using this method, they successfully analysed Fe_2O_3 with a FeO standard.

Other approaches to the analysis of first row transition metals have been tried. Gopon *et al.* [28] analysed Fe silicides using the Fe-Lℓ noting that unlike the Fe-Lα and -Lβ X-ray lines it was not affected by bonding. This method has yielded improved quantification compared to using the Fe Lα-line without correcting for bonding effects. Statham and Holland [7] tested the Lℓ-line for measurement of steels, again finding improved quantification compared to Lα, although Cr-Lℓ was 9 % relative below the expected value. The Lℓ typically has low intensity compared to the Lα-, Lβ-lines limiting sensitivity and precision [7, 28]. Another solution is the use of calibration curves, allowing the use of the higher intensity Lα- and Lβ-lines whilst avoiding a knowledge of the variation in MACs and fluorescence yields, such as demonstrated by Buse and Kearns [29] for olivine. Moy and Fournelle [30] have investigated the use of non-machine specific calibration curves, by using the integrated intensity across

the Lα- and Lβ-emission lines. The calibration curve is material specific, in this case Fe-silicides. Errors using a machine specific calibration curve are < 3.6 % relative, excluding two samples which are believed to be tilted.

2. Achieving high spatial resolution for Fe-bearing minerals

Fe-bearing minerals demonstrate the problems in analysing first row transition metals at high resolution. In this section, we analyse Fe-bearing minerals using the two strategies outlined above. To address the problems of L-line analysis several approaches are used: (1) Fe-Lℓ analysis, (2) calibration curve for Fe-Lα analysis when re-peaking on each sample, (3) calibration curve for Fe-Lα analysis with a fixed position, and (4) extending the method of Buse and Kearns [25] using a regression-fit to experimentally measured MACs and calculated partial fluorescence corrections to cover silicate minerals with complex substitutions and varying oxidation states. Measurements were made on a JEOL 8530F FEG EPMA at the University of Bristol. A Peltier cold finger [19] was used during analysis to minimise contamination and analyses were widely spaced to avoid carbon contamination from previous points. The measurements were made using a 10 μm beam size to avoid the possibility of eroding the carbon coat, thereby allowing the ability of quantification procedures to be assessed whilst removing other affects.

2.1. Fe-Kα low overvoltage measurements

Analysing the Fe Kα-line with an accelerating voltage of 10 kV, gives an overvoltage of 1.4 and yields low ionisation with net counts ca. 100 cps/nA on Fe metal using LIF compared to 1,200 - 1,600 cps/nA at 20 kV for the same crystals. Comparable precision therefore requires longer count times and/or higher beam currents. High precision was obtained for the measurements e.g., 0.8 % rel. (2 σ) for St John's Island Olivine with 7.5 wt% Fe, using a high beam current (100 nA) and long count times (60 seconds on peak) and two spectrometers combined. The results are shown in Fig. 5, comparing measured values to reference values. The results are accurate to within 5 % relative and generally insensitive to the choice of standard.

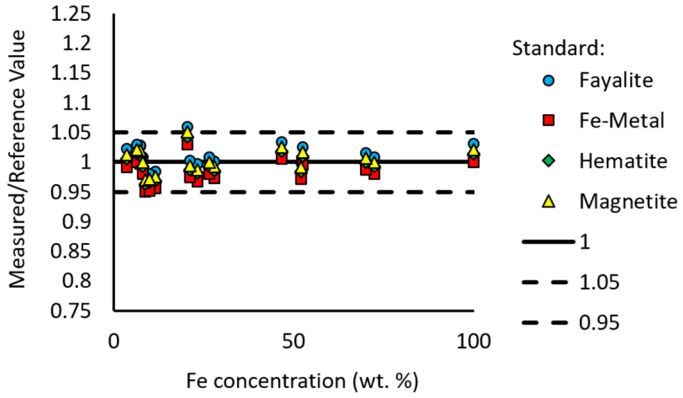

Figure 5. Fe-Kα measurements at 10 kV compared to reference values, using 4 different materials as a standard.

2.2. Fe-Lℓ measurements

The Fe Lℓ-line was measured at 7 kV, 200 nA for 120 seconds on peak using a TAPH crystal. Careful background selection is required to avoid interference with Fe-Lη and Mn-Lα peaks; in this case only the upper background measurement was used. Fe-Lℓ has low net intensities of 4.37 cps/nA on Fe metal. This is primarily a function of the refracting crystal, for despite the low fluorescence yield of L3-shell vacancies, this is compensated by the large number of ionisations. L3-shell vacancies are either filled by electrons from the M5-shell to yield Lα X-rays, or the M1-shell to yield Lℓ X-rays. Lα X-rays dominate, although the relative intensity depends on the occupancy of the 3d electron shell, which varies with element [31, 32] and bonding.

The low intensities are reflected in the larger errors at the low concentrations (Fig. 6a). The accuracy of the results varies considerably between samples, with some samples differing from reference values by > 5 % relative. The calculated concentrations are sensitive to the standard used (Fig. 6b), with magnetite standard giving the best results for the dataset, whilst Fe metal performing poorly. A look at the peak positions for fayalite and Fe metal shows that this poor performance is not due to peak shift or shape.

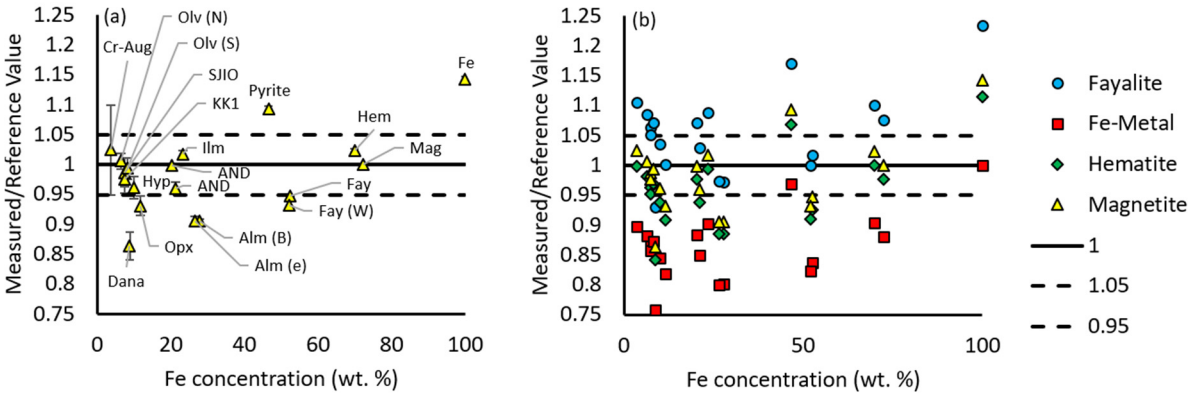

Figure 6. Fe-Lℓ measurements at 7 kV compared to reference values using a) magnetite, and b) 4 different materials as the standard. 1 sigma error bars shown for (a).

2.3. Fe-Lα measurements using calibration curves

Fe Lα was measured at 7 kV, 200 nA, on a TAP crystal, counting for 60 seconds on peak. Two methods of measuring the Fe Lα-line were tested, one using a fixed peak position (that of Fe metal), the other peaking up on each sample. To understand the changes in peak position, Fig. 7 shows the shift in peak positions (see [33]). The Lα-peak position shifts to high wavelengths with increasing Fe content as the low wavelength side is strongly absorbed by the Fe-L3 absorption edge. As Hofer and Brey [34] for garnets and Fialin *et al.* [33] for a range of minerals have shown Fe self-absorption is greatest for Fe^{2+}, with Fe^{3+} resulting in a shift in the absorption edge away from the Lα-peak maximum. Therefore, as Fialin *et al.* [33] showed, on Fig. 7 the samples with Fe^{3+} have peak positions at lower wavelengths consistent with less self-absorption.

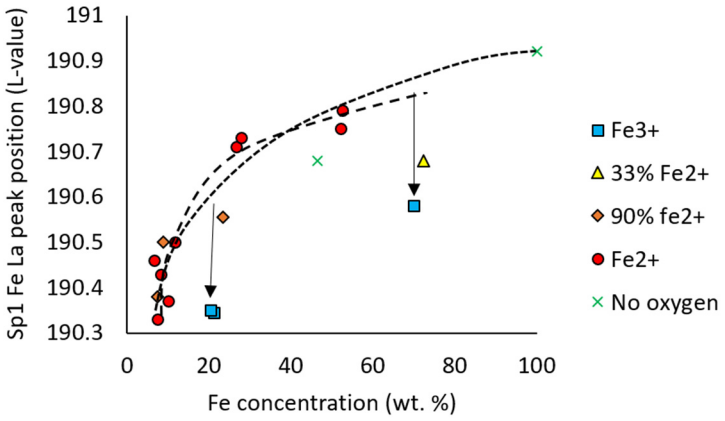

Figure 7. Fe Lα-peak, colour coded in terms of their Fe oxidation state. There is uncertainty where to plot the trend line, and whether it is continuous with Fe metal.

Figures 8 and 9 give the results for Lα using re-peaking on each sample and a fixed position. To interpret the results we must consider the measurement position relative to the peak maximum, the true emission peak position (the peak maximum without self-absorption), and the position of absorption maximum. In Fig. 8 each measurement is at peak maximum, but the peak maximum moves away from the true emission peak (and the absorption maximum) as absorption erodes the low wavelength side of the peak. In Fig. 9 the measurements are at the Fe metal peak, which is easy to accurately define, and reflects the emission peak for Fe metal. However, whilst this is close to the peak maximum for the minerals with high Fe content (see Fig. 7) as a result of absorption eroding the high-energy side of the peak, it is a long way from the true emission peak, approximated by the low Fe content samples which have suffered less absorption (see Fig. 7, also [25, 33]). The Fe peak position, has lower energy than the absorption edge for both Fe^{2+}- and Fe^{3+}-minerals, making absorption similar at this position. Both datasets show a tendency for calculated *k*-ratios to overestimate, particularly at high concentrations where self-absorption is higher. This corresponds to elevated MACs for minerals containing oxygen compared to Fe metal, consistent with the findings of Buse and Kearns [25] and Moy and Fournelle [35] for olivine. The opposite is seen for pyrite (FeS_2), where the calculated *k*-ratio underestimates, this is consistent with pyrite having a lower MAC than Fe metal, similar to that observed by Llovet *et al.* [24] for Ni-silicides.

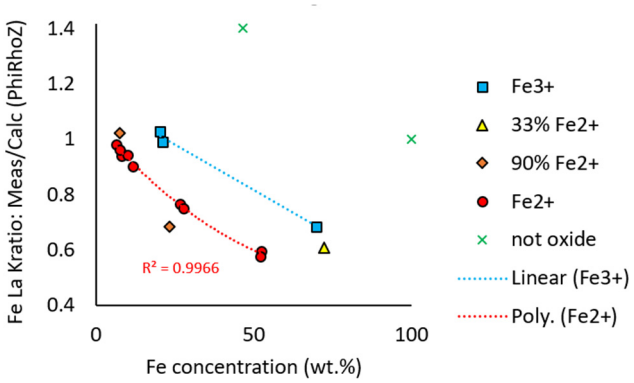

Figure 8. Fe-Lα measurements, on peak maximum, with peak search for each sample. Colour coded for Fe chemical state.

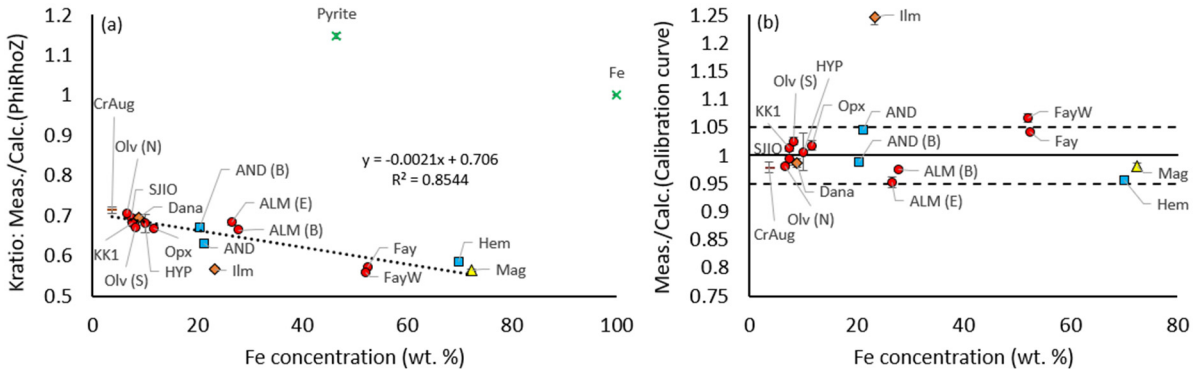

Figure 9. Fe-Lα measurements using the Fe metal peak position. a) Measured *k*-ratios compared to calculated *k*-ratios using phi-rho-Z models. Regression does not include pyrite and Fe metal; b) Measured *k*-ratios compared to calculated *k*-ratios using a calibration curve, here pyrite and Fe are off-scale. 1 sigma error bars are plotted. Colours and symbols are the same as for Figs. 8 and 7 and correspond to Fe chemical state. Cr-Augite has 80 % Fe^{2+}.

If we compare the two sets of measurements, it can be seen that by re-peaking on each sample, the discrepancy between measured and calculated *k*-ratios is largely removed for minerals with low Fe-content, where measurement is now close to the true emission peak and absorption is minimal. At high Fe contents, re-peaking has little effect, as the peak maxima are close to Fe metal. Crucially whilst measurement using peak maximum differentiates between Fe^{2+}- and Fe^{3+}-minerals and is, therefore, sensitive to the differences in self-absorption with Fe valence state; measurement at the Fe-metal peak position is not sensitive to this. This appears to result from the measurement being acquired below the absorption edge for both Fe^{2+}- and Fe^{3+}-minerals, resulting in similar absorption. This approach was tested on an extended range of minerals shown in Fig. 10, in this case to achieve similar precision correction for matrix effects from the other elements was required.

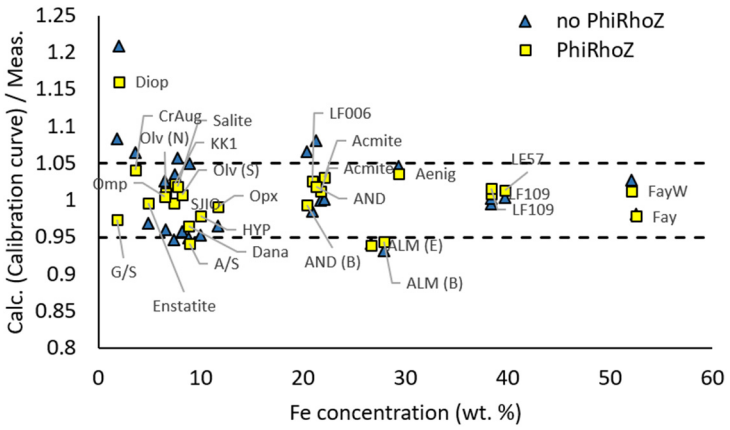

Figure 10. Measurements at the Fe metal peak (as in Fig. 9) for an extended range of materials. Agreement between measured values and calculated values using a calibration curve is improved when correcting for the matrix effects on Fe from the other elements in the material. Minerals include: pyroxences (CrAug, enstatite, diop, hyp, salite, acmite), olivines (Olv(N), Olv(S), LF57, LF109, LF006, SJIO), garnets (AND, ALM, G/S, A/S, Dana), aenigmatite (Aenig) and amphiboles (Omp, KK1).

2.4. Fe Lα measurements: experimental MACs and partial fluorescence yields

To investigate the application of the method of Buse and Kearns [25] to a range of silicate minerals with different valence states, MACs were measured for a range of materials (Fig. 11a). MACs were measured using the procedure outlined in Buse and Kearns [25], based on the method of Pouchou and Pouchoir [22], whereby the MAC is varied until a good agreement is reached between measured and calculated values for a range of voltages. It can be seen from Fig. 11a, that the MAC for Fe-Lα by Fe is a function of valence state, consistent with the observations above. Coordination does not appear to have a strong effect. Therefore, if the valence state is known, the MAC can be calculated. To determine the valence state, the ratio of Lα to Lβ at fixed positions was used as a proxy, as shown in Fig. 11b. This allows the MAC to be calculated from the Lα/Lβ-ratio and the Fe concentration.

Figure 12a shows the calculated partial fluorescence yield correction. Partial fluorescence yields were calculated using the method of Pouchou and Pouchoir [22] and Llovet et al. [24]. The calculated partial fluorescence yields appear to vary as a function of Fe concentration, with oxidation state having minimal influence. By using the experimentally measured MACs and the calculated partial fluorescence yield corrections, concentrations were calculated to within ± 10 % relative of the expected values (Fig. 12b).

3. Discussion

The measurements made for Fe using the Kα X-ray at low overvoltage and L-line X-rays at low voltage provide us with a good position for examining the various options for high spatial resolution and their merits. The Fe-Kα measurements gave the most reliable results both accurate and precise for all the materials measured including both pyrite and Fe metal. The measurements were also insensitive to the standard used. The limitation being that whilst the spatial resolution for Fe-Kα measurments at 10 kV

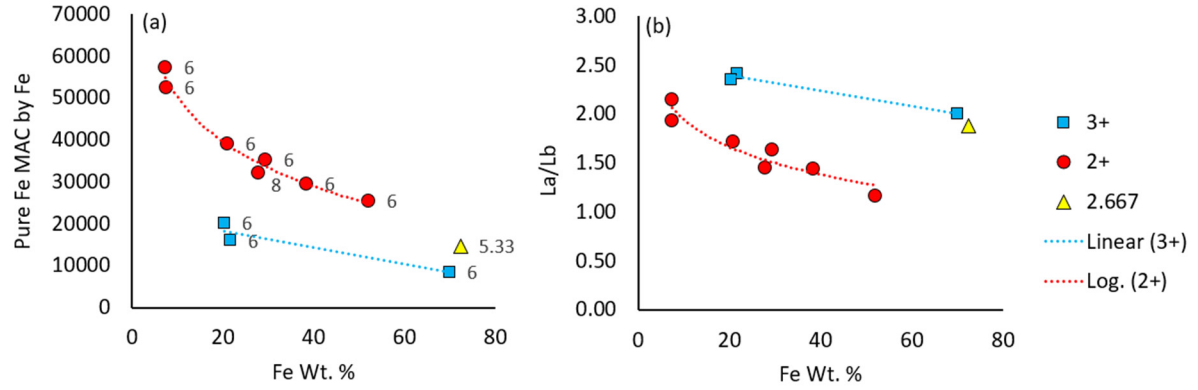

Figure 11. a) Experimentally measured MACs for Fe-Lα by Fe, and b) measurements of Lα/Lβ-ratio for materials with varying Fe oxidation state (colours - see legend), and coordination number (labels on a).

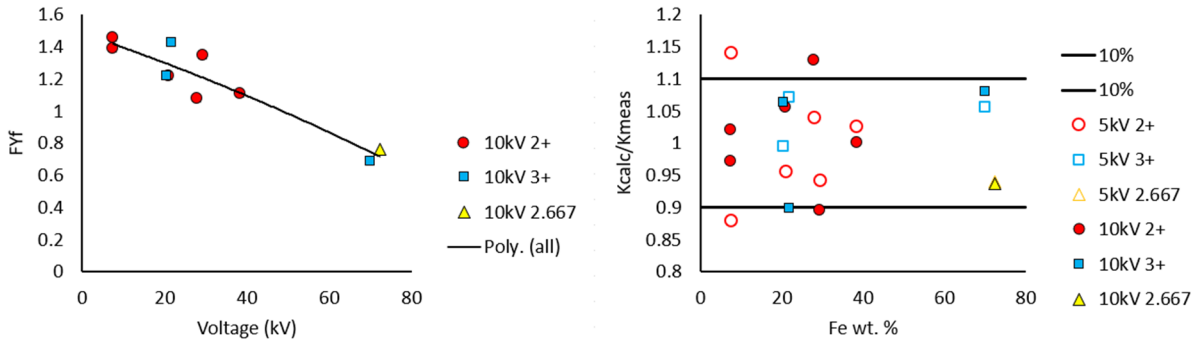

Figure 12. a) Variations in partial fluorescence yield, and b) agreement between calculated and measured *k*-ratios using calculated partial fluoresecence yields and mass absorption coefficients for the range of samples.

is very good (depth < 350 nm for ulvospinel, Fig. 1) to achieve a similar resolution for the other elements such as Si or more usefully Mg, Al and Ti in the case of ulvospinel, measurement at several voltages is required (as given in Table 1). To achieve high lateral resolution a small spot size is required. At 10 kV, 100 nA beam current, a spot size of 100 nm can be achieved [3]. This degrades the lateral resolution by ca. 100 nm (see Fig. 2) making it significantly worse than the depth resolution. Poorer lateral resolution is acceptable for polished cubic phases where the depth is typically substantially less than the width. At small spot sizes and high power, there would be the potential for carbon erosion - this should be assessed and if necessary, a correction applied using TDI. Alternatively, a different coating material may be used.

The measurement of Fe using L-line X-rays allows measurement at low voltage providing high spatial resolution (< 350 nm depth at 7 kV for ulvospinel, Fig. 1) for all the X-rays which can be excited. The results show, in keeping with previous findings (e.g., [7, 28]), that the Lℓ-line provides reasonable results (accuracy within ≤ 10 % relative), which is a substantial improvement from conventional Lα-line measurements for first row transition metals. The Lℓ measurements clearly require careful selection of the standard, with this having a significant effect on accuracy. Errors are large at low concentrations due to the weak intensity of this line. The intensity of the Lℓ-line relative to Lα varies with element, becoming more favourable as the atomic number is reduced towards Ti and the occupancy of the 3d

shell declines reducing L3-M5 transitions [31, 36]. The results show that whilst conventional Lα measurements are highly inaccurate (with discrepancies up to 45 % relative) the use of a calibration curve to calculate Fe concentration can yield good results with accuracy approximating ≤ 5 % for a range of minerals (excluding Fe metal, pyrite and ilmenite) and are rendered insensitive to Fe oxidation state when a fixed position is used. Whilst this accuracy is less than achieved in standard high voltage analysis (typically 1 - 2 % relative) and is less robust than the low overvoltage measurements made using the Fe-Kα X-ray line, it is a significant result. The accuracy is comparable to measurements made of olivine where the solid-solution MACs and partial fluorescence yields were determined [25], achieving accuracies of ≤ 4 %. The main advantage of this calibration curve approach is the ability to measure a range of minerals (olivine, pyroxene, garnet, and some oxide minerals) of varying oxidation state. Simple solid-solution MACs are unable to account for the variations in MAC with Fe valence changes. Initial tests in calculating MACs and partial fluorescence yields for a range of silicate minerals with varying oxidation states, are encouraging but require further investigation to see if similar precision can be achieved. If we consider the lateral resolution for the Lα calibration curve method; at 200 nA and 7 kV the spot size would exceed 150 nm [3], making the lateral resolution worse than the depth resolution. At 7 kV carbon coat erosion is expected to be worse [14], although the effect on X-ray intensities may be similar or less given the larger overvoltages. Again, TDI or other coating materials could be considered. Improvements to the Fe-L depth resolution could be made by dropping the accelerating voltage, but below 4.97 kV Ti-K cannot be excited, and with reduction in voltage there is an associated increase in spot size, particularly at high beam currents [3].

In the above cases, use of high beam currents (100 nA - 200 nA) are necessary to provide high precision. To achieve higher lateral resolution by reducing spot sizes lower beam currents could be used. For Fe Kα at low overvoltage the higher intensities would permit a reduction in beam current whilst still maintaining reasonable precision (e.g., 1.6 % relative 2σ for St John's Island olivine with 7.5 wt% Fe at 25 nA using 2 spectrometers), although trace element sensitivity would be reduced. In both the case of Lα X-rays and even more so using Lℓ X-rays, the lower X-ray intensities using a TAP crystal limit the potential for reducing the beam current whilst maintaining reasonable precision. While many mineral species are stable under the electron beam (e.g., olivine, pyroxene, garnet and spinel), it is not true for others minerals such as carbonates, phosphates, micas and natural glass. In the case of plagioclase feldspar the resolution achievable is significantly affected by the stability of the sample requiring a defocussed beam. Saunders *et al.* [37] found that while a spatial resolution of ≤ 350 nm could be achieved for orthopyroxene with a 30 nm beam at 5 kV, plagioclase required a 500 nm defocussed beam yielding a spatial resolution of ca. 750 nm to maintain sample stability.

4. Conclusions

The optimum analytical conditions for a given analysis are complex to determine and the maximum spatial resolution achievable is dependent on the elements and material analysed. Low overvoltage and low voltage provide two mechanisms of achieving high resolution, with the resolution a function of the electron range, the spot size and the overvoltage and absorption of a particular element (e.g., [3, 4]). The spot size depends on the precision and sensitivity required, together with the intensity of an X-ray line on a particular diffraction crystal. Maximum spatial resolution will be achieved for major element analysis of X-ray lines > 1 keV, where low beam currents can be used in combination with low overvoltage or low voltage settings, for dense materials (e.g., [1]).

The measurements demonstrate that low overvoltage measurements can give robust results, regardless of the material being analysed, but are limited to one or a few elements at a given voltage. Low overvoltage analysis is very sensitive to carbon erosion which occurs at high current density, and carbon contamination, which is especially problematic for tightly spaced analyses. Robust results require mitigation or avoidance of these affects. Mitigation methods include TDI correction and the use of other coating materials for carbon erosion [14] and the use of an anticontamination cold-finger and

empirical corrections for contamination [17]. Depending on the sample, the use of an oxygen air-jet, stage heating, chamber plasma cleaning or sample preparation using FIB milling or argon cross-section polishing may be suitable to reduce contamination [17-21].

Low voltage analysis provides high spatial resolution for all the X-rays excited, equal or less than the interaction volume. It does however restrict the X-rays which can be used. The L-line X-rays of transition metals are particularly problematic. The Fe-Lα measurements show that despite anomalous absorption and partial fluorescence yields (see [24]), reasonably accurate results can be obtained using either a calibration curve for a range of minerals, or experimentally determined solid-solution MACs and partial fluorescence yields for a single mineral solid solution [25]. Initial application of experimentally determined MACs and partial fluorescence yields for a range of silicate minerals are encouraging, but currently yield larger errors. The calibration curve using the Fe metal peak position provides a method of measurement which removes sensitivity to Fe valence state. A consequence of using the TAP crystal for L-line measurements is the low intensity, requiring high beam currents for high precision particularly at low concentrations, thereby limiting the lateral resolution through larger spot sizes. The choice of low overvoltage or low voltage L-line method will therefore depend on the precision and accuracy required and the material analysed, with L-lines requiring a range of standards for calibration curves, or pre calculated solid solution MACs and partial fluorescence yields.

Acknowledgments
We would like to thank the Smithsonian Institute for supplying the Rockport, Fayalite standard (NMNH 85276).

References

[1] Kimura T, Nishida K and Tanuma S 2006 *Microchim. Acta* **155** 175-178
[2] Hovington P, Drouin D and Gauvin R 1997 *Scanning* **19** 1-14
[3] Pinard P T and Richter S 2014 *IOP Conf. Ser.: Mater. Sci. Engng.* **55** 012016
[4] McSwiggen P 2014 *IOP Conf. Ser.: Mater. Sci. Engng.* **55** 012009
[5] Llovet X and Salvat F 2016 *IOP Conf. Ser.: Mater. Sci. Engng.* **109** 012009
[6] Ritchie N W 2009 *Microsc. Microanal.* **15** 454-468
[7] Statham P and Holland J 2014 *IOP Conf. Ser.: Mater. Sci. Engng.* **55** 012017
[8] Kubo Y, Hamada K and Urano A 2003 *Ultramicroscopy* **135** 64-70
[9] Bastin G F and Heijigers H J M 1990 *Scanning* **12** 225-236
[10] Chopra D 1970 *Phys. Rev. A* **1** 230-235
[11] Fischer D W and Baun W L 1967 *J Appl. Phys.* **38** 4830-4836
[12] Lábár J L and Salter C 1991 in: *Electron probe quantitation*. (Heinrich K F J and Newbury D E; Eds.). (New York, NY: Plenum Press) 223
[13] Matthews M B, Kearns S L and Buse B 2018 *Microsc. Microanal.* **24** 83-92
[14] Matthews M B, Kearns S L and Buse B 2018 *Microsc. Microanal.* **24** 612-622
[15] Matthews M B, Kearns S L and Buse B 2019 *Microsc. Microanal.* **25** 1112-1129
[16] Pinard P T, Schwedt A, Ramazani A, Prahl U and Richter S 2013 *Microsc. Microanal.* **19** 996-1006
[17] Buse B and Kearns S 2015 *Microsc. Microanal.* **21** 594-605
[18] Bastin G F and Heijligers H J M 1988 in: *Microbeam analysi*s. (Newbury D E; Ed.). (San Francisco, CA: San Franciso Press) 325
[19] Buse B, Kearns S, Clapham C and Hawley D 2016 *Microsc. Microanal.* **22** 981-986
[20] Augustyn E, Hallstedt B, Wietbrock B, Mayer J, Schwedt A and Richter S 2012 *IOP Conf. Ser.: Mater. Sci. Engng.* **32** 012001
[21] Yamashita T, Tanaka Y, Yagoshi M and Ishida K 2016 *Sci. Rep-UK* **6** 29825
[22] Pouchou J L and Pichoir F 1985 *J. Microsc. Spectrosc. Electron.* **10** 291-294
[23] Fialin M 1990 *X-ray Spectrom.* **19** 169-172

[24] Llovet X, Pinard P T, Heikinheimo E and Louhenkilpi S 2016 *Microsc. Microanal.* **22** 1233-1243
[25] Buse B and Kearns S L 2018 *Microsc. Microanal.* **24** 1-7
[26] Moy A and Fournelle J 2018 *Microsc. Microanal.* **24** (Suppl. 1)
[27] Rémond G, Myklebust R, Fialin M, Nockolds C, Phillips M and Roques-Carmes C 2002 *J. Res. Natl. Inst. Stand. Technol.* **107** 509-529
[28] Gopon P, Fournelle J, Sobol P E and Llovet X 2013 *Microsc. Microanal.* **19** 1698-1708
[29] Buse B and Kearns S L 2011 in: *Book of Abstracts of the European Microbeam Analysis Society 12th European Workshop*. (Angers, France; 15-19 May)
[30] Moy A and Fournelle J 2019 *Microsc. Microanal.* **25** 664-674
[31] Wyckoff R W G and Davidson F D 1965 *J. Appl. Phys.* **36** 1883-1885
[32] Okada M 1981 *J. Radioanal. Chem.* **63** 201-204
[33] Fialin M, Wagner C, Métrich N, Humler E, Galoisy L and Bézos A 2001 *Amer. Mineralogist* **86** 456-465
[34] Hofer H E and Brey G P 2007 *Amer. Mineralogist* **92** 873-885
[35] Moy A and Fournelle J 2017 *Microsc. Microanal.* **23** (Suppl. 1)
[36] Holliday J E 1962 *J. Appl. Phys.* **33** 3259-3265
[37] Saunders K, Buse B, Kilburn M R, Kearns S and Blundy J 2014 *Chem. Geol.* **364** 20-32